Published in final edited form as:
J Mol Biol. 2008 January 11; 375(2): 572–580. doi:10.1016/j.jmb.2007.10.052.

A kinetic intermediate that regulates proper folding of a group II intron RNA

Christina Waldsich[1,†] and **Anna Marie Pyle**[1,2,*]

[1]Department of Molecular Biophysics and Biochemistry, Yale University, New Haven, CT 06520, USA

[2]Howard Hughes Medical Institute, Yale University, New Haven, CT 06520, USA

Summary

The D135 group II intron ribozyme follows a unique folding pathway that is direct and appears to be devoid of kinetic traps. During the earliest stages of folding, D135 collapses slowly to a compact intermediate, and all subsequent assembly events are rapid. Collapse of intron Domain 1 (D1) has been shown to limit the rate constant for D135 folding, although the specific substructure of the D1 kinetic intermediate has not yet been identified. Employing time-resolved Nucleotide Analog Interference Mapping (NAIM), we have identified a cluster of atoms within the D1 main stem that control the rate constant for D135 collapse. Functional groups within the κ–ζ element are particularly important for this earliest stage of folding, which is intriguing given that this same motif also serves later as the docking site for catalytic Domain 5 (D5). Importantly, the κ–ζ element is shown to be a divalent ion binding pocket, indicating that this region is a Mg^{2+}-dependent switch that initiates the cascade of D135 folding events. By measuring the Mg^{2+} dependence of the compaction rate constant, we conclude that the actual rate-limiting step in D1 compaction involves the formation of an unstable folding intermediate that is captured by the binding of Mg^{2+}. This carefully orchestrated folding pathway, in which formation of an active-site docking region is early and rate-limiting, ensures proper folding of the intron core and faithful splicing. It may represent an important paradigm for the folding of large, multidomain RNA molecules.

Keywords

ribozyme; RNA folding; catalysis; splicing; RNA structure

INTRODUCTION

Highly specific architectural forms are required for RNA molecules to accomplish their many tasks in the cell. In order to reach their native, functional states, RNA molecules must traverse a variety of possible folding landscapes that depend on sequence and environmental conditions [1; 2; 3; 4; 5]. Although the individual characteristics of such landscapes are of great interest, one of the most intriguing aspects of an RNA folding pathway is the nature of the rate-limiting step. In many cases, escape from a kinetic trap is rate-limiting, whereby stable alternative

*corresponding author: Anna Marie Pyle, Department of Molecular Biophysics and Biochemistry, Yale University, 266 Whitney Ave., New Haven, CT 06520; phone: +1 203 432 5633; fax: +1 203 432 5316; email: anna.pyle@yale.edu.
†present address: Department of Biochemistry, MFPL, University of Vienna, Dr. Bohrgasse 9/5, 1030 Vienna, Austria

conformations present obstacles along the folding pathway [1; 2]. Alternatively, folding of a large RNA can be slowed by extensive conformational searching, as tertiary interaction partners attempt to find each other [6]. Finally, the formation of unstable and highly specific substructures can delay the folding process [3; 7].

The D135 group II intron ribozyme traverses a highly unusual folding landscape that has underscored the potential diversity in RNA folding mechanisms [8; 9; 10; 11; 12]. This RNA folds directly to the native state through a series of on-pathway intermediates [13]. Although D135 does not become kinetically trapped [10], the early stages of its tertiary structural collapse are very slow [9]. The rate constant for folding is limited by the formation of the scaffolding domain (D1), whereas the subsequent docking of catalytic domains D3 and D5 is very fast [9]. The tertiary collapse of D1 requires magnesium [9], and it is stabilized by an unusual substructure in the central stem of D1 [11]. Despite these new insights into the folding mechanism, the nature of the rate-limiting event remains enigmatic.

In this work, we used time-resolved Nucleotide Analog Interference Mapping (NAIM) in conjunction with native gel electrophoresis to identify the intron functional groups that influence the rate-limiting step for tertiary collapse of D135. Surprisingly, most of the NAIM effects cluster within the small κ-ζ substructure in D1, suggesting that this motif forms a kinetic intermediate along the D135 folding pathway. Our data further suggests that the κ-ζ substructure is a Mg^{2+}-dependent switch that is essential for initial stages of molecular collapse. Importantly, this same motif also controls the stability of D135 compaction [11] and anchors the active site during final stages of intron assembly.

RESULTS

Experimental design

To identify individual functional groups that contribute to the rate-limiting step for D135 tertiary compaction (defined specifically as the molecular collapse from the secondary structure to the tertiary structure), we developed a selection that is based on the time-dependence of D135 compaction. In an adaptation of NAIM [14] (Figure 1), D135 RNA was transcribed in the presence of nucleotide analogs resulting in a pool of D135 molecules that contain random, single-atom modifications. This pool of RNAs was rapidly mixed with 100 mM Mg^{2+} (to initiate tertiary folding) and allowed to incubate for short times prior to electrophoretic separation of the folded and unfolded populations (Figure 1). The success of this technique was dependent on a highly stringent selection step, in which the pool of modified RNAs is allowed only a brief period of time to compact (approximately the $t_{1/2}$ for compaction [9], which is 15-45 seconds, depending on the analog). Note that the timescale for D135 collapse is slightly and reproducibly faster than the timescale for native state formation (2 min^{-1} vs. 1 min^{-1})[9; 10], which suggests that the system is not perfectly two-state. This allows a small amount of collapsed intermediate state (rather than native state) to accumulate at very short times[9]. The pool is almost completely folded at incubation times of approximately 1 minute (data not shown), which strongly suggests that the system is under kinetic selection. After isolating the folded and unfolded populations from the gel, iodine sequencing was used to identify the sites of modification that were most disruptive to the kinetics of D135 collapse.

Notably, a similar electrophoretic approach was previously used to determine the functional groups that control the magnesium-dependent stability of D135 folding at equilibrium [11]. In that previous case, the modified pool of D135 was incubated for longer times (10 min) at very low magnesium ion concentrations (4-6 mM), which provides a stringent selection for stabilizing functional groups. While this experiment enabled us to acquire information on thermodynamic determinants for folding, it was not designed to reveal RNA substructures that

are important for the kinetic folding pathway or to reveal information on kinetic barriers to the native state.

The κ–ζ element in the D1 central stem controls the time-scale for the tertiary collapse

All of the time-resolved NAIM signals are located within D1 (Figure 2), which is consistent with D1 compaction as the rate-limiting step in folding of the D135 ribozyme [9]. Among the observed effects are a few interferences at residues that participate in long-range intradomain interactions, such as α-α' and β-β' [15; 16]. While these tertiary contacts may assist in D135 folding, their lower abundance suggests that they are not of primary importance for the rate-limiting step of compaction.

The strongest interferences and enhancements were clustered primarily within the D1 central stem, in the vicinity of a substructure known as the κ–ζ element. Nucleotides in this region displayed strong phosphorothioate and 2'deoxynucleotide effects (Figures 2 and 3; Supplementary Figure 1). In addition, the relative sensitivity of specific nucleobase functional groups indicates that local duplex stability of this region is vital for D135 compaction. This is indicated by N6-methylAαS and IαS interferences as well as DAPαS enhancements (Figures 2 and 3; Supplementary Figure 1). Many terminal base-pairs appear to be involved in tertiary contacts or in non-canonical reverse Hoogsteen base pairings, as indicated by 7-deazaAαS and N6-methylAαS interferences (e.g. A191-U390 or A205-U212). NAIM patterns within the κ–ζ region itself are largely inconsistent with a GNRA-like fold for κ or a receptor-like fold for ζ in the kinetic intermediate (compare NAIM signatures in Figure 2 with [17]).

The interferences and enhancements identified using time-resolved NAIM are in close agreement with the NAIM effects observed for tertiary collapse during equilibrium folding [11]. Of the few differences between the two studies (~10% of the total number of NAIM effects), only 3 affect the κ–ζ element: A376 and A378 exhibit an additional 2' OH interference, but A378 lacks the weak 7-deazaAαS interference in the time-resolved NAIM assay. Other deviations between the two NAIM approaches are located at residues part of or close to the long-range tertiary interactions α–α' and β–β' (e.g. a 2'OH interference at G145, IαS interference at G316, or N6-methylAαS enhancement at A336 detected in this study). The striking correlation between the two NAIM studies indicates that the same D1 substructure controls both the timescale and stability of intron collapse, which has important implications for the folding mechanism.

The κ–ζ element contains a divalent ion binding pocket

The numerous phosphorothioate effects in the κ–ζ region suggest that metal ions may be involved in folding and anchoring of this site. Nonetheless, a previous analysis of Tb^{3+}-induced cleavage did not reveal any apparent Mg^{2+} ion pockets within the κ–ζ region [18]. This result does not preclude the existence of a metal ion binding site, however, as Tb^{3+} cleavage requires that the nucleophilic 2'OH group must become perfectly aligned for attack (a condition met primarily in dynamic loop structures [18]). There are other limitations to the use of Tb^{3+} for probing the location of metal ion binding sites. For example, metal ions interacting with the major groove of RNA cannot be detected using this assay and hydrogen bonding to 2'-OH groups at the scissile site will prevent Tb^{3+}-cleavage. Differences in valence, ionic radius and pK_a value can also prevent Tb^{3+} from binding to a Mg^{2+} site.

Previous Tb^{3+} analyses had been conducted on the tightly-packed native state of D135 [18]. We reasoned that the D135 structure might be more flexible in the intermediate state, in which only D1 has collapsed. The 2'OH groups near κ–ζ might be more accessible and dynamic, resulting in additional cleavages by bound Tb^{3+}. To test these ideas, the Tb^{3+} assay was adapted to study metal-ion induced cleavage of D135 molecules in both the intermediate collapsed state and the

native state (Figure 4). D135 was folded under low magnesium ion conditions that allow D1 collapse (10 mM; close to the K_{Mg} of compaction), and in high magnesium ion conditions that promote formation of the fully native conformation (100 mM)[9; 10]. Indeed, distinct Tb^{3+}-cleavage patterns were observed specifically at the κ–ζ element in the intermediate state (Figure 4), but not the high-magnesium native state, as described previously [18]. Importantly, the κ–ζ element is the only region of the molecule that is more highly cleaved by Tb^{3+} in the intermediate state than in the native state, which indicates that Tb^{3+} does not simply increase overall background cleavage for the intermediate state. These data suggest that the κ–ζ element binds metal ions and that this process makes an important contribution to compaction. Cleavage is observed over a range of residues within the κ–ζ element, which suggests that this region has an increased backbone flexibility in the intermediate state and that it may also have a significantly larger electronegative potential than surrounding substructures in D1.

The Mg^{2+}-dependence of compaction kinetics

Although the previous results underscore the importance of Mg^{2+} in formation of the κ–ζ element, they do not define the role of Mg^{2+} in the kinetic mechanism of compaction. To address this issue, we examined the Mg^{2+} dependence of D135 compaction kinetics. In a range of [Mg^{2+}] that spans the K_{Mg} for compaction (5-30 mM), the rate constant for compaction stays relatively constant (~ 0.15 min^{-1}), indicating that Mg^{2+} binding is not the actual rate-limiting step. However, the amplitude for compaction extent is dependent on Mg^{2+}, increasing from 24% at 5 mM Mg^{2+} to 60% at 30 mM (Table 1, Supplementary Figure 2). When reaction amplitude, but not the rate constant, is dependent on ligand concentration, a conformational capture mechanism is implicated [19]. In this case, the D1 main stem appears to stochastically sample the "correct" conformation over some rate-limiting timescale. However, this "correct" conformation is unstable, and must be trapped by Mg^{2+} binding, resulting in a reaction amplitude that is directly proportional to Mg^{2+} concentration. Mg^{2+} capture of the κ–ζ element induces the D1 collapse, which is then likely to be completed by the formation of long-range tertiary interactions within D1, which is consistent with the weak NAIM signals observed in these regions.

Formation of specific helical elements is Mg^{2+}-dependent

Certain NAIM effects indicate that formation of specific secondary structures also plays a key role in tertiary collapse (e.g. helix d and d'' or stem a; Figure 2). This is somewhat surprising given that the "unfolded" state in this study is defined as an RNA that has already been preincubated with monovalent ions and is therefore electrostatically relaxed. Much of the secondary structure has already formed and the RNA has undergone a partial structural collapse that is evident as a decrease in molecular radius (R_H)[8].

To rigorously characterize the secondary structure of the "unfolded state" and to determine which helices have already formed, we performed DMS (dimethyl sulfate) structural probing on D135 that had been preincubated only in KCl. DMS modifies the N1 atom of adenine and the N3 atom of cytidine residues that are not involved in Watson-Crick base pairing or other forms of hydrogen bonding. The DMS accessibility patterns indicate that most of the D135 secondary structure is formed in the unfolded state, but no tertiary contacts have formed (e.g. α-α' or ζ-ζ' interactions; Figure 5). However, certain adenines and cytidines remain highly accessible to DMS (Figure 5 and Supplementary Figure 3), including nucleotides that normally encompass helical stems d, d', d" and d'" in the fully-folded structure. Notably, these helices are comprised of residues with a high contact order, which will increase the complexity of the conformational search involved in their formation. In addition, the formation of D1 stems a, b and c is also dependent on divalent ions. These data indicate that nucleotides in the central D1 stem, which spans the κ–ζ element, are disordered in the unfolded state and that Mg^{2+} is important for organization of the entire central stem.

To further investigate the Mg^{2+}-dependence of helices that facilitate D135 collapse, we conducted an additional DMS interference analysis on the compact intermediate state. In an approach similar to equilibrium NAIM analysis [11], D135 was modified with DMS and the pool was allowed to fold under low magnesium ion concentrations that are just below the K_{Mg} for molecular compaction. As in equilibrium NAIM analyses [11], this provides a stringent selection against functional groups that interfere with Mg^{2+}-dependent compaction. This approach resulted in DMS interferences and enhancements in the same regions previously identified by equilibrium NAIM (compare Figure 5 with Figure 2 and [11]). Of particular importance is that interferences were observed for A (N1) and C (N3) residues that are contained within helices of the D1 central stem. These sites (e.g. A195 and A196 in stem d or A219 and A220 in stem d") correspond with NAIM N6-methylAαS interferences (Figure 2), which are also markers for duplex structure. Thus, local duplex stability seems to be a crucial determinant for D135 compaction. The results suggest that D1 collapse depends on a collaborative interplay of secondary and tertiary structural features and that it is mediated by Mg^{2+} stabilization of the κ–ζ element.

DISCUSSION

Despite the emergence of diverse paradigms for describing pathways of RNA tertiary folding, we know little about the structural features of RNA folding intermediates [20]. Considerable attention has been focused on the features of kinetically trapped structures (i.e. misfolded RNAs [1]). However, to understand the driving forces for native RNA structures, it is essential to characterize the properties of obligate folding intermediates that lie on the tertiary folding pathway. Given that the D135 group II intron ribozyme folds directly to the native state, it provides a valuable system for investigating the structural features of obligate folding intermediates.

In this study, we employed a kinetic selection in order to identify specific functional groups that control the rate-limiting step in group II intron folding. It is highly significant that the results were not deduced from equilibrium measurements, but from methods that are sensitive to transient intermediates along the dynamic folding pathway. Despite the vast size of the intron, we observe that its folding kinetics is controlled by a small substructure in the main stem of D1, known as the κ–ζ region. This ensemble of loops and helices behaves as a kinetically controlled, Mg^{2+}-dependent switch, and collapse of the entire intron is predicated on the proper formation of this motif. Remarkably, this motif has a second function during the final stages intron assembly, where it serves as the docking site for catalytic domain 5.

These data and previous results [13] are consistent with a model that explains the remarkable accuracy and the slow rate constant observed for D135 folding. Upon addition of Mg^{2+}, folding of D135 is initiated from a state in which all of the secondary structure has formed except for duplexes in the D1 central stem. In the earliest and slowest stage of folding, the κ–ζ element and surrounding duplexes coalesce into a unique structural state that is stabilized by Mg^{2+} and which results in a specific orientation of flanking helices. Once this architecture has been established, long-range tertiary interaction partners that span the central stem can snap together and lock the D1 structure into its collapsed form (such as α–α' and β–β', which are sites of weak NAIM signals). Similarly, once D1 has formed the collapsed scaffold (which faithfully occurs in isolated D1 molecules), intron catalytic domains 3, 5 and 6 rapidly dock into place, resulting in the catalytically active, native state. The coordinated stages of this ordered pathway are likely to reduce the formation of misfolded structures, to facilitate proper folding of the intron core and therefore to promote faithful splicing.

It is important to consider why consolidation of κ–ζ and its surrounding helices is slow and rate-limiting for the process of folding. While an answer to this question will depend on detailed

biophysical analyses of this minimal region, some insights into this problem have already been obtained. First of all, it is unlikely that consolidation of κ–ζ is limited by the rate constant for escaping a misfolded intermediate (a kinetic trap). A kinetic trap model for D135 is inconsistent with urea-independence and other attributes of the pathway that are observed both at 42°C and at 30°C, at a diversity of ionic conditions ([13], C.W. and A.M.P, unpublished). Data from a variety of experiments, including DMS footprinting studies on the unfolded state (Figure 4) indicate that the challenge to D135 folding is not the hyperstabilization of structure, but a lack of stability in the D1 central stem.

Indeed, an alternative mechanism is suggested by experiments that monitor the magnesium dependence of the compaction rate constant (Table 1): The rate constant for compaction does not decrease upon the addition of Mg^{2+} (as is common for kinetically trapped species [21; 22]). Rather, it remains constant with increasing [Mg^{2+}] while compaction amplitude increases. This suggests that the active conformation of κ–ζ and surrounding duplexes is slowly sampled and is ultimately captured by the binding of Mg^{2+}. Given that helices embedding the κ–ζ element are formed by residues with high contact order, it is possible that a conformational search limits the rate constant for the formation of the D1 main stem and the κ–ζ substructure, which is ultimately trapped by the binding of Mg^{2+} (a conformational capture mechanism [19]). Mg^{2+} binding then stabilizes the κ–ζ region and neighboring substructures, thereby inducing D1 collapse.

Although this model provides an appealing way to describe stabilizing ligand binding to a dynamic RNA molecule, it may not be ideal for describing systems in which the ionic strength is very high and the ligand in question is Mg^{2+}. In such cases, the local concentration of Mg^{2+} may not increase with the bulk Mg^{2+} indefinitely, and may plateau at a value that is influenced by local electrostatic properties of the RNA. Thus, it is possible that the rate constant for folding might saturate with Mg^{2+} concentration even without the capture of an ion to a specific site. Put simply, the effect of metal ion concentration on folding kinetics is not well understood and may represent a more complex problem than a binding event involving Mg^{2+} association with a specific RNA motif. Another important consideration is that the concentration of Mg^{2+} *in vivo* is insufficiently high to serve as the ligand for stabilization of the κ–ζ substructure. In a physiological environment, this role is probably played by associated proteins, such as Mss116p, which is required for ai5γ splicing in yeast and under near-physiological conditions *in vitro* 13.

It is highly significant that the NAIM patterns observed in this kinetic analysis are similar to those reported in a previous equilibrium study of D135 compaction [11]. The parity in results from the two studies indicates that the first structural element that folds during tertiary collapse is the same motif that is most critical for stabilizing the ground-state for compaction. This is not necessarily expected: For example, formation of long-range interactions such as α–α' could have been rate-limiting events, with core stability mediated by separate elements. In addition, it was highly unexpected that the same D1 folding element would be identified in studies that utilized high and low magnesium ion concentrations, as other RNA molecules undergo a fundamental shift in folding mechanism under different ionic conditions. The parity in results between the two studies provides important evidence for the proposed folding mechanism. In this process, the same RNA functional groups that contribute to rate-limiting formation of the critical folding intermediate are also important for binding the Mg^{2+} ions that are essential for stability of the compact state.

Although the folding mechanism of D135 appears to be completely distinctive, there are similarities with other RNA systems. For example, tertiary folding of D135 is unusual in that the slowest stage occurs early in the process and subsequent domain docking events are fast. The slow stage involves formation of an obligate substructure that requires magnesium binding

for stability. This mechanism is a mirror image of behavior observed for the catalytic domain from RNAse P. In that case, initial phases of tertiary collapse are fast, whereas the final stage of folding is slow and it involves the Mg^{2+}-dependent stabilization of a small RNA substructure [3]. These systems demonstrate that similar types of folding intermediates can dominate the kinetic pathway at different stages of the overall mechanism (i.e. at the beginning or at the end) [13]. Through structural characterization of these intermediates, we may gain valuable insights into the driving forces for RNA tertiary structure formation.

MATERIALS AND METHODS

Nucleotide Analog Interference Mapping

The experimental setup and quantitation of NAIM effects was similar to that described previously [11], although short reaction times provided the selective pressure for tertiary collapse: The 5' or 3' labeled RNAs were denatured at 95°C for 1 minute in the presence of 0.5M KCl and 80mM MOPS pH 7.0. After cooling the samples, $MgCl_2$ was added to a final concentration of 100mM and samples were allowed to fold for 15 to 45 seconds at 42°C followed by immediate loading on a 6% native polyacrylamide gel that contained 4mM Mg^{2+}. Native gel electrophoresis for the selection and for study of compaction kinetics was conducted described previously [9; 11].

Tb^{3+}-induced cleavage

The 5' labeled D135 RNA was denatured for one minute at 95°C in a buffer containing 0.5 M KCl and 80mM MOPS pH 7.0. After cooling to room temperature, D135 was folded by adding 10mM or 100mM $MgCl_2$ and incubating at 42°C for one hour. $TbCl_3$-cleavage was then performed as previously described [18], whereby increasing amounts of $TbCl_3$ (0.01-2.5mM, Sigma) was added to the samples.

DMS (Dimethyl sulfate) interference analysis

Cold D135 RNA (5nM) was combined with trace concentrations of 5' labeled D135 RNA and denatured in a buffer of 0.5M KCl and 80mM potassium cacodylate, pH 7.0. After cooling, the sample was equilibrated at 42°C for 10 minutes. Subsequently, the RNA was modified with DMS (10.7mM) at room temperature for 20 minutes followed by quenching with β-mercaptoethanol. The DMS modified RNA was denatured at 95°C for 1 minute in the presence of 0.5M KCl and 80mM MOPS pH7. Then 15mM $MgCl_2$ was added and the sample was incubated at 42°C for 10 minutes. After folding the RNA was loaded on a 6%-10mM Mg^{2+} native gels [23] in order to separate the unfolded and folded populations, which were excised from the gel, eluted and examined by reverse transcription [24]. Given that the RT primer hybridizes to the 3'-terminus of D135, it was not possible to analyze the entire span of D5 for potential interferences (A827 is the first mapped residue). Although D5 was not included into the summary map (Figure 5), interferences were not detected within readable sequence that spans this domain (G815 to A827).

Supplementary Material

Refer to Web version on PubMed Central for supplementary material.

Acknowledgments

We would like to acknowledge Olga Fedorova for many helpful discussions and for critically reading the manuscript. Roland Sigel is also thanked for helpful discussions. We thank Gabriele Drews is for excellent technical assistance. This work was supported by NIH grant GM50313 (to A.M.P) and by a schrödinger postdoctoral fellowship (J2332) from the Austrian Science Foundation (to C.W). A.M.P. is an investigator of the Howard Hughes Medical Institute.

References

1. Treiber DK, Williamson JR. Exposing the kinetic traps in RNA folding. Curr Opin Struct Biol 1999;9:339–345. [PubMed: 10361090]
2. Treiber DK, Williamson JR. Beyond kinetic traps in RNA folding. Curr Opin Struct Biol 2001;11:309–314. [PubMed: 11406379]
3. Sosnick TR, Pan T. RNA folding: models and perspectives. Curr Opin Struct Biol 2003;13:309–316. [PubMed: 12831881]
4. Schroeder R, Barta A, Semrad K. Strategies for RNA folding and assembly. Nat Rev Mol Cell Biol 2004;5:908–919. [PubMed: 15520810]
5. Woodson SA. Structure and assembly of group I introns. Curr Opin Struct Biol. 2005
6. Sosnick TR, Pan T. Reduced contact order and RNA folding rates. J Mol Biol 2004;342:1359–65. [PubMed: 15364565]
7. Woodson SA. Folding mechanisms of group I ribozymes: role of stability and contact order. Biochem Soc Trans 2001;30:1166–9. [PubMed: 12440997]
8. Su LJ, Brenowitz M, Pyle AM. An alternative route for the folding of large RNAs: apparent two-state folding by a group II intron ribozyme. J Mol Biol 2003;334:639–652. [PubMed: 14636593]
9. Su LJ, Waldsich C, Pyle AM. An obligate intermediate along the slow folding pathway of a group II intron ribozyme. Nucleic Acids Res 2005;33:6674–87. [PubMed: 16314300]
10. Swisher JF, Su LJ, Brenowitz M, Anderson VE, Pyle AM. Productive folding to the native state by a group II intron ribozyme. J Mol Biol 2002;315:297–310. [PubMed: 11786013]
11. Waldsich C, Pyle AM. A folding control element for tertiary collapse of a group II intron ribozyme. Nat Struct Mol Biol 2007;14:37–44. [PubMed: 17143279]
12. Fedorova O, Waldsich C, Pyle AM. Group II intron folding under near-physiological conditions: collapsing to the near-native state. J Mol Biol 2007;366:1099–1114. [PubMed: 17196976]
13. Pyle AM, Fedorova O, Waldsich C. Folding of group II introns: a model system for large, multidomain RNAs? Trends Biochem Sci 2007;32:138–45. [PubMed: 17289393]
14. Strobel SA. A chemogenetic approach to RNA function/structure analysis. Curr Opin Struct Biol 1999;9:346–52. [PubMed: 10361087]
15. Harris-Kerr CL, Zhang M, Peebles CL. The phylogenetically predicted base-pairing interaction between a and a' is required for group II splicing *in vitro*. Proc Natl Acad Sci USA 1993;90:10658–10662. [PubMed: 7504276]
16. Michel F, Ferat J-L. Structure and activities of group II introns. Annu Rev Biochem 1995;64:435–461. [PubMed: 7574489]
17. Boudvillain M, Pyle AM. Defining functional groups, core structural features and inter-domain tertiary contacts essential for group II intron self-splicing: a NAIM analysis. EMBO J 1998;17:7091–7104. [PubMed: 9843513]
18. Sigel R, Vaidya A, Pyle A. Metal ion binding sites in a group II intron core. Nat Struct Biol 2000;7:1111–6. [PubMed: 11101891]
19. Weeks KM, Cech TR. Assembly of a ribonucleoprotein catalyst by tertiary structure capture. Science 1996;271:345–348. [PubMed: 8553068]
20. Baird NJ, Westhof E, Qin H, Pan T, Sosnick TR. Structure of a folding intermediate reveals the interplay between core and peripheral elements in RNA folding. J Mol Biol 2005;352:712–22. [PubMed: 16115647]
21. Pan J, Thirumalai D, Woodson S. Magnesium-dependent folding of self-splicing RNA: exploring the link between cooperativity, thermodynamics, and kinetics. Proc Natl Acad Sci U S A 1999;96:6149–54. [PubMed: 10339556]
22. Rook MS, Treiber DK, Williamson JR. An optimal Mg(2+) concentration for kinetic folding of the tetrahymena ribozyme. Proc Natl Acad Sci U S A 1999;96:12471–6. [PubMed: 10535946]
23. Pyle AM, McSwiggen JA, Cech TR. Direct measurement of oligonucleotide substrate binding to wild-type and mutant ribozymes from *Tetrahymena*. Proc Natl Acad Sci USA 1990;87:8187–91. [PubMed: 2236030]

24. Konforti BB, Liu Q, Pyle AM. A map of the binding site for catalytic domain 5 in the core of a group II intron ribozyme. Embo J 1998;17:7105–17. [PubMed: 9843514]

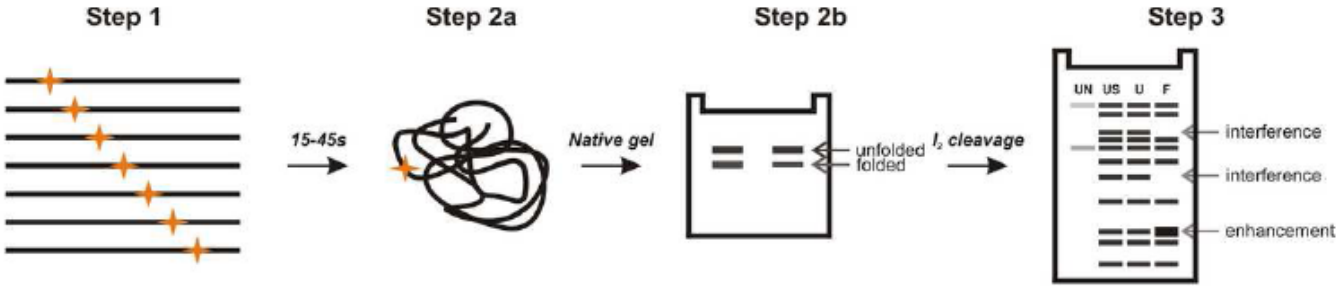

Figure 1. Experimental set up

Scheme of the individual steps involved in mapping the functional groups important for compaction of the *Sc*. ai5γ D135 ribozyme. Gold stars indicate the incorporation of a nucleotide analog.

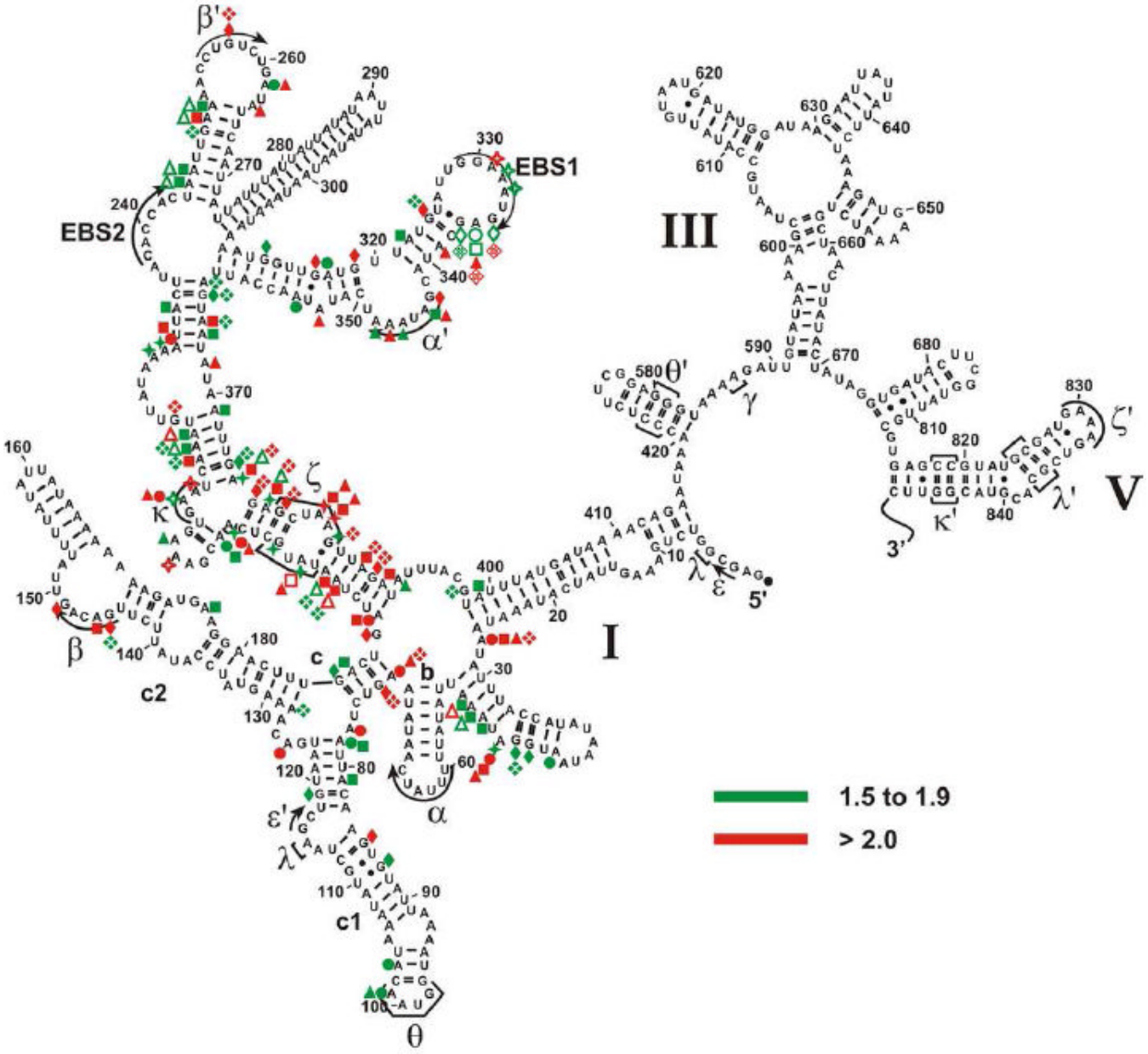

Figure 2. Functional groups important for the tertiary collapse

Strong interferences and enhancements are shown in red (2 to 5.2), while weak interferences and enhancements are displayed in green (1.5 to 1.9). The various symbols reflect different analogs: AαS or GαS analog (star), 7-deazaAαS (sphere), N6-methylAαS (square), DAPαS (triangle), 2'dAαS or 2'dGαS analogs (grid) and IαS (diamond). Open symbols represent enhancements and closed symbols indicate interferences.

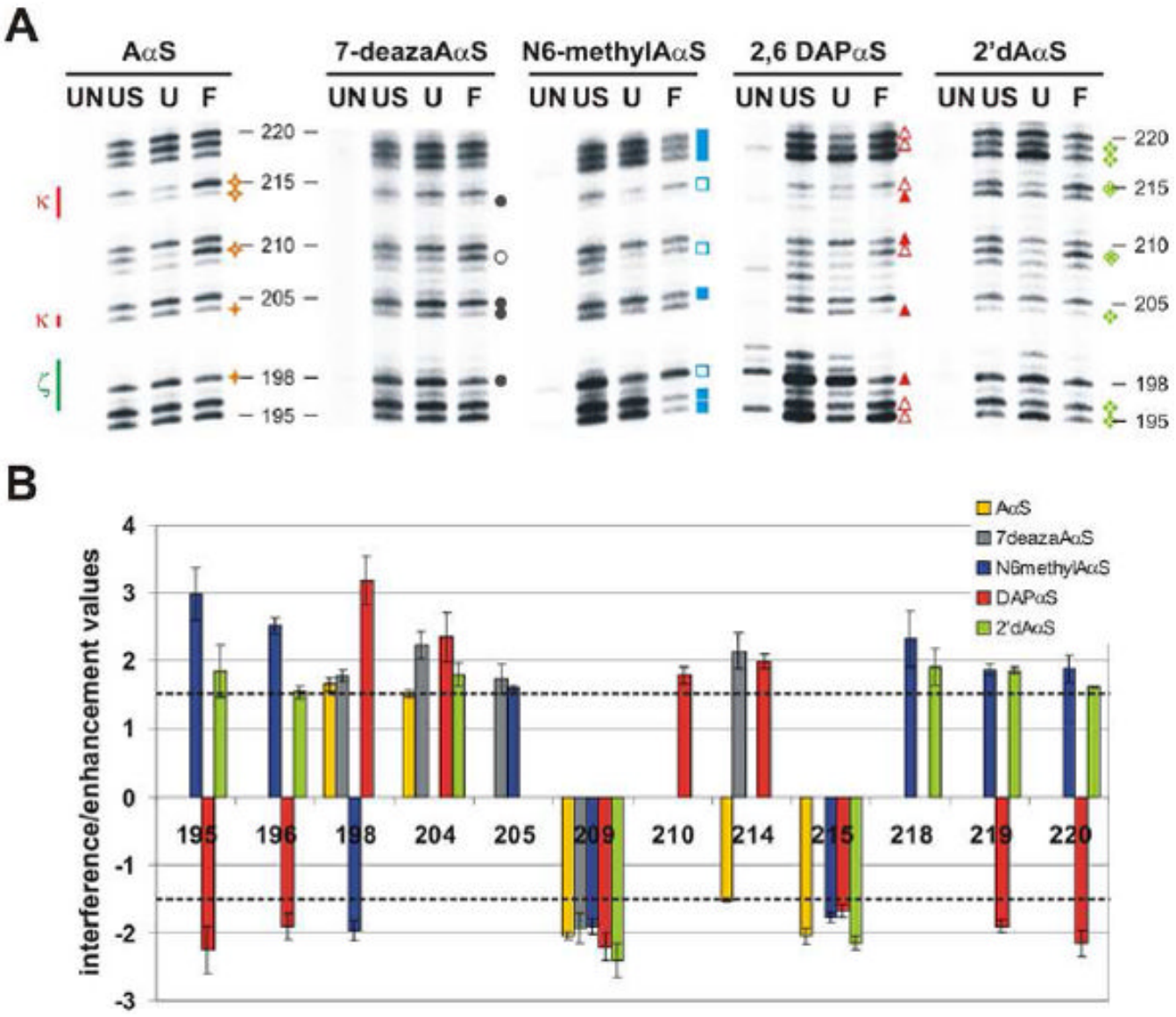

Figure 3. The D5 docking site in domain 1

(a) Representative gels depict the 5' regions of the D5 docking site comprising the κ–ζ element. For each gel lane 1 (UN) shows the background degradation of the labeled RNA, while lane 2 (US) represents the relative incorporation level for an analog at a specific position (RNA, which did not undergo the selection step, was iodine cleaved). Lane 3 (U) shows iodine cleavage products for RNA, which stems from the unfolded population purified from the native gel. Lane 4 (F) shows iodine cleavage products for RNA, which stems from the folded population eluted from the native gel. The NAIM effects of different backbone or nucleobase substitutions are shown in distinct colors: AαS or GαS analog (dark yellow), 7-deazaAαS (gray), N6-methylAαS (blue), DAPαS (red), 2'dAαS or 2'dGαS analogs (light green) and IαS (purple). Symbols used in this figure are explained in the legend to Figure 2. (b) Bar diagram displays the average value and standard deviation for each interference and enhancement found within the 5' regions of the D5 docking site (except for G200). The dotted line indicates the cutoff below which interferences and enhancements were considered insignificant.

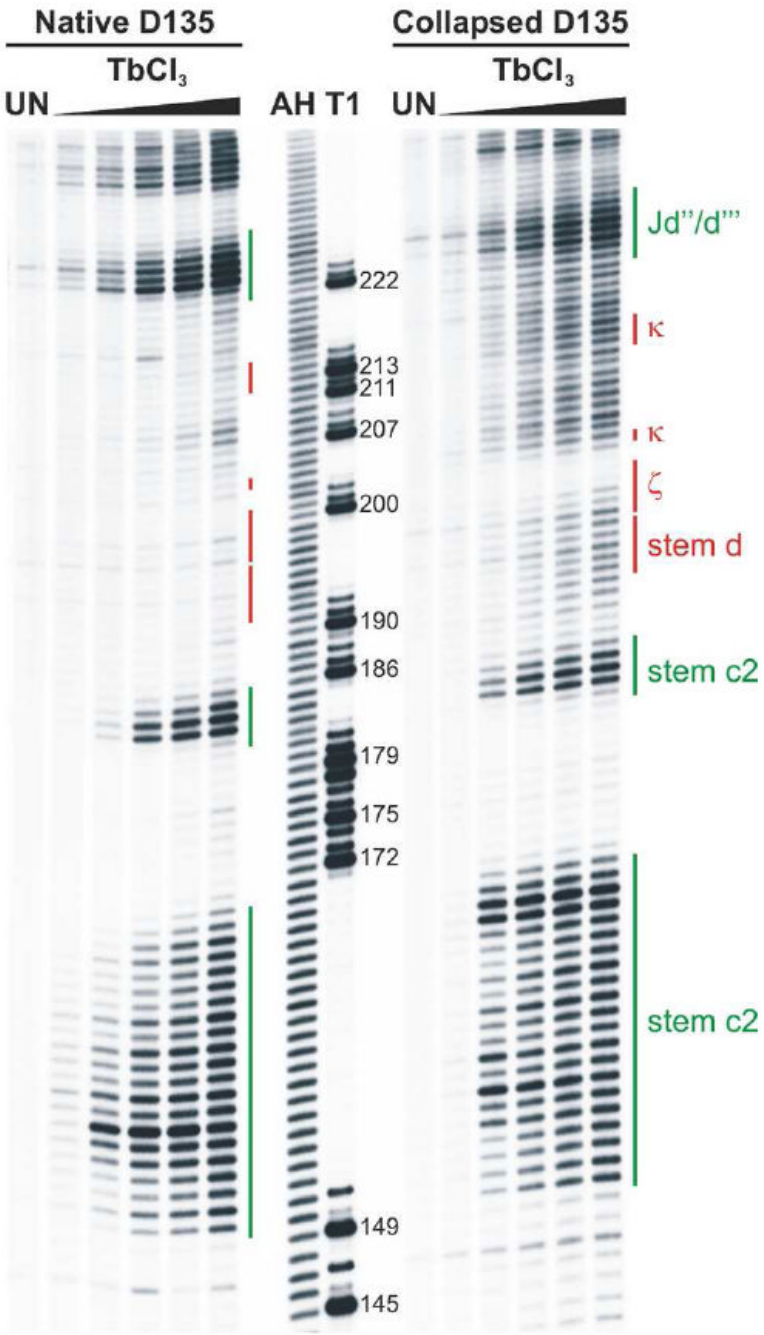

Figure 4. Metal ion-induced cleavage in the compact versus the native D135 ribozyme

The left panel shows the Tb^{3+}-induced cleavage pattern observed for the native D135 ribozyme and the right panel displays that of the collapsed D135 ribozyme. Lanes designated as UN show background degradation of the labeled RNA. The T1 lane marks the guanosine sequencing lane, while lane AH is the alkaline hydrolysis ladder. Bars on the side of each gel span residues part of a particular structural element, which is also identified on the right panel, whereby the D5 docking site is marked in red and other elements are labeled in green.

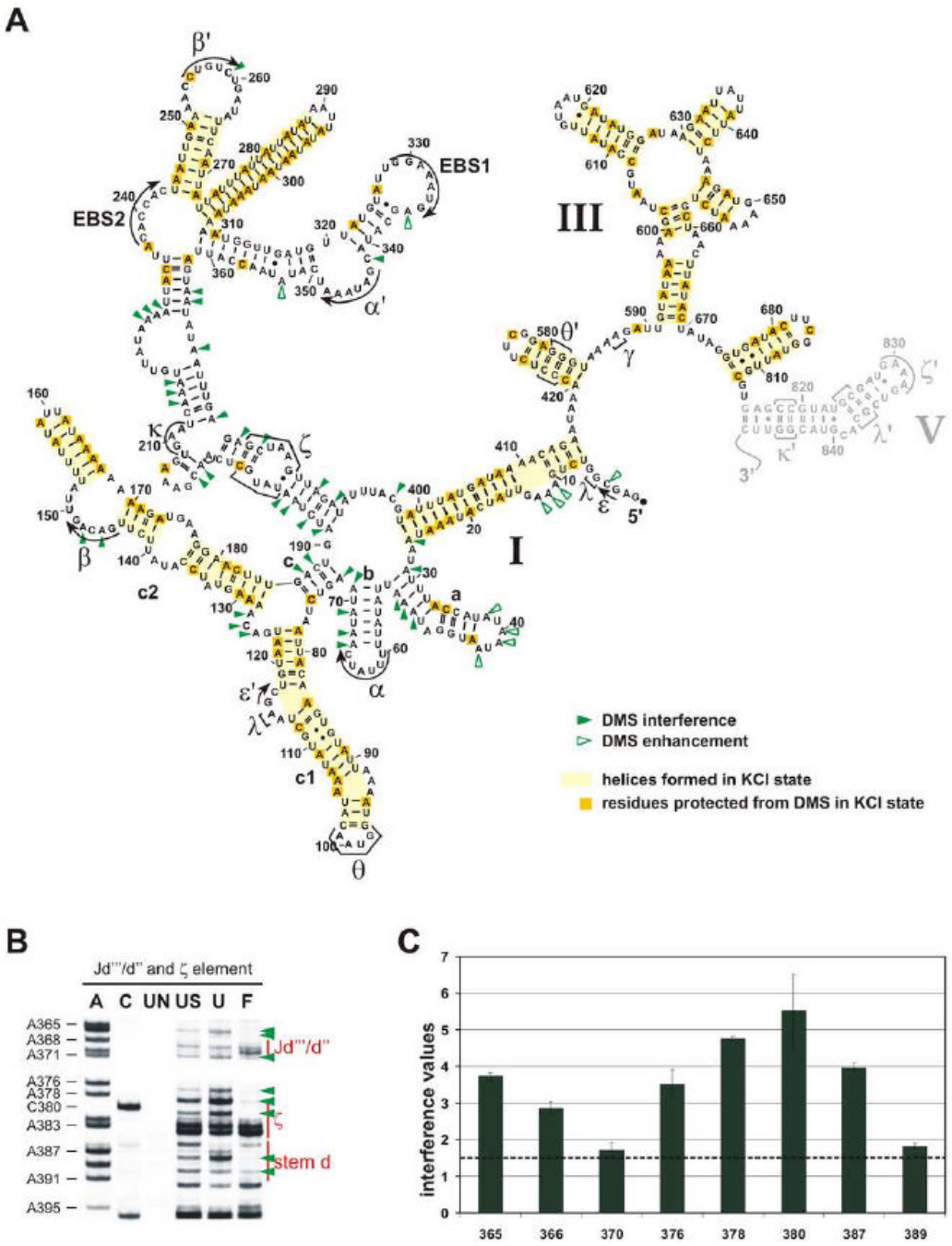

Figure 5. Formation of some secondary structure depends on divalent ions and is important for the tertiary collapse of the Sc. ai5γ *D135* ribozyme

(a) The 'KCl state' and a summary map of observed DMS interferences and enhancements. Helical structures formed in the absence of any divalent ions (unfolded state) are highlighted in yellow (darker yellow boxes indicate the A and C residues that were not methylated by DMS). Green arrowheads mark the observed DMS interferences (closed symbol) or enhancements (open symbol). D5 is marked in gray, because it was not included in the analysis (see Methods). (b) Representative gels for the D5 docking site (ζ element) and flanking regions. The abbreviation scheme (UN, US, U, F) was explained in the legend to Figure 3; A and C refer to the sequence lanes which are required to identify the sites of interference. (c) Bar

diagram shows the average value and standard deviation for each interference and enhancement found within the region shown in (b). The dotted line indicates the cutoff below which interferences and enhancements were considered insignificant.

Table 1

The rate of compaction of the D135 ribozyme is compared at various Mg^{2+} concentrations

Average values and standard deviations for the rate-constants and amplitudes were calculated from at least six independent experiments.

Mg^{2+} [mM]	k_{comp} [min^{-1}]	amplitude [%]
5	0.10 ± 0.02	24 ± 2
10	0.14 ± 0.05	39 ± 3
15	0.18 ± 0.05	40 ± 12
20	0.13 ± 0.03	51 ± 10
30	0.22 ± 0.05	60 ± 5